ELSEVIER

Physica B 296 (2001) 129–137

PHYSICA B

www.elsevier.com/locate/physb

Tight-binding Hamiltonians for realistic electronic structure calculations☆

Dimitrios A. Papaconstantopoulos[a,b,*], Mohammed Lach-hab[b], Michael J. Mehl[a]

[a]*Center for Computational Materials Science, Naval Research Laboratory, Washington, DC 20375-5345, USA*
[b]*School of Computational Sciences, George Mason University, Fairfax, VA 22030-4444, USA*

Abstract

This article, written in honor of Eleftherios N. Economou, contains a short summary of work one of us carried out some 20 years ago in collaboration with Lefteris and reports on recent developments on the use of tight-binding Hamiltonians to perform accurate and efficient electronic structure calculations. More specifically, in this work we use the newly developed NRL tight-binding method to explore the existence of metastable phases in transition metals, present new Slater–Koster parametrizations of cubic perovskite materials and provide an extension of the Slater–Koster approach that includes the spin–orbit interaction.

Keywords: Electronic structure; Tight binding

1. Background – reminiscences

Since this volume is written in honor of Professor Economou, we shall preface our contribution with a short account of work one of us (DAP) did with him utilizing a tight-binding (TB) formalism. We first developed an accurate TB parametrization of Si [1]. This involved an orthogonal sp Hamiltonian that included 20 three-center Slater–Koster (SK) parameters which extended to third nearest-neighbor distances. The SK parameters were fitted to accurately reproduce local pseudopotential results provided by Pickett. We obtained an excellent fit to the valence bands as well as the first two conduction bands and a band gap of 1 eV. We then applied this Hamiltonian to the problem of the ideal vacancy in Si. An important issue at that time was to determine the position of the bound state within the energy gap. Using the Green's function G that corresponds to the TB Hamiltonian we found that the real part of G as a function of energy goes to zero at a value of 0.75 eV above the top of the valence band in agreement with more elaborate self-consistent calculations. In subsequent work [2,3] we used the same Hamiltonian for Si with the addition of Si–H and H–H matrix elements to generate a model for hydrogenated amorphous Si. In this work we employed the coherent potential approximation (CPA) and demonstrated the appearance of states in the gap due to dangling

☆Proceedings of the E.N. Economou Symposium on "Wave Propagation and Electronic Structure in Disordered Systems", Physica, 2001.

*Corresponding author. Present address: Center for Computational Materials Science, Naval Research Laboratory, Washington, DC 20375-5345, USA. Fax: +1-202-404-7546.

E-mail address: papacon@dave.nrl.navy.mil (D.A. Papaconstantopoulos).

0921-4526/01/$ - see front matter
PII: S0921-4526(00)00790-0

bonds and the restoration and widening of the band gap with increasing hydrogen content. In further work [4] with Warren Pickett we used a Kubo–Greenwood formula to calculate the optical absorption. We found that the optical gap is larger than the calculated density of states gap and agrees well with experimental data. These results suggested that the optical absorption is determined primarily by the local H–Si configuration and short-range order, but that it is insensitive to the long-range order.

In Section 2 of this paper we present a summary of the tight-binding work performed at NRL and an application to the problem of metastable structures. In Section 3 we concentrate in examining the Slater–Koster methodology for multi-atom systems of the perovskite structure and in Section 4 we present an extension of the SK approach that incorporates spin–orbit interactions. A summary is given in Section 5.

2. Further developments on tight-binding Hamiltonians

The work for Si described in the previous section is based on a SK parametrization in an orthogonal three-center TB formulation. In later years DAP produced SK parameters for most elements in the periodic system and extended the work to include two center integrals as well as non-orthogonal basis [5]. This work provides a very good description of the energy bands and the densities of states of many materials. In recent work Mehl and DAP [6] have succeeded in fitting not only the band structure but the total energy as well. This has been accomplished by writing the SK parameters in polynomial form, providing a bond length dependence to the hopping integrals and a local density dependence to the on-site terms. This scheme, called the NRL–TB method, has also been programmed to do molecular dynamics simulations for systems close to 1000 atoms and for a few thousand steps. This task is beyond the means of first-principles methods such as the full potential linearized augmented plane wave (LAPW) or linearized muffin-tin orbital (LMTO) [7]. This method ensures transferability of the SK parameters from one structure to another and provides the means to calculate elastic constants, phonon spectra, vacancy formation, surface energies and stacking fault energies very efficiently (i.e. at least 1000 faster than LAPW calculations). This approach is based on an original database of energy bands and total energies generated by first-principles calculations (in our case LAPW) as a function of volume for a few high symmetry structures, such as FCC and BCC. This method is suitable to handle accurately both metals and non-metals as well as ferromagnets. For details of the NRL–TB method the reader is referred to Ref. [6]. An extension of this method to spin-polarized calculations is presented in this volume in the article by Bacalis et al. [8].

To demonstrate one of the capabilities of the NRL–TB method we present here some new results on the question of the metastability of the BCC and HCP phases. It is well known that the FCC transition metals have significantly lower melting temperatures than both the BCC and HCP metals. On the other hand the FCC metals are ductile while the BCC metals are brittle. It is, therefore, of technological interest to investigate the possibility that the BCC or the HCP metals have a metastable FCC phase. In Fig. 1 we show the energy–strain relationships of the BCC metals from which one derives the elastic constants C_{11}–C_{12} and C_{44} calculated in the FCC lattice. We note that with the exception of Fe, which is known to have a metastable FCC phase, these metals show energy–strain graphs with a negative slope which will result in negative elastic constants, indicating the instability of the FCC phase for V, Nb, Ta, Mo and W. It should be stressed here that the results for Fe shown in Fig. 1 correspond to paramagnetic calculations which have the FCC as the ground state [6]. A similar plot in Fig. 2 summarizes our calculations for the metals whose ground state is HCP. We note that all of these metals have positive elastic constants suggesting that a metastable FCC phase is expected. This is confirmed experimentally at least for Sc and Y [9].

We have also calculated the Bain path for all transition metals. Our general conclusion is that for those metals that have an FCC ground state the BCC lattice is unstable. The reverse is true for the BCC metals as stated above.

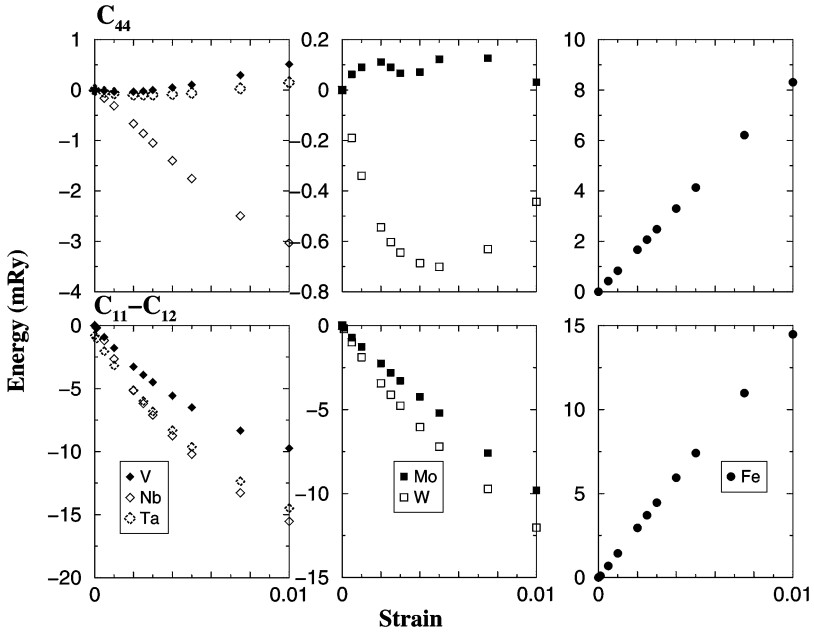

Fig. 1. Energy versus strain relationship for the BCC transition metals computed in an assumed FCC lattice. Only FCC Fe appears to be metastable.

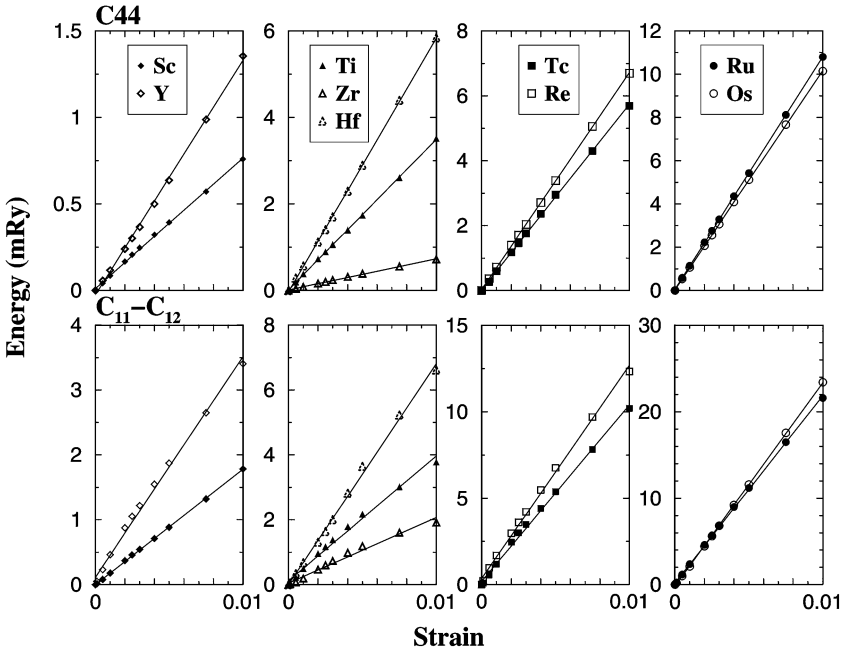

Fig. 2. Energy versus strain relationship for the HCP transition metals computed in an assumed FCC lattice. They all show potentially metastable FCC structures.

3. Cubic perovskite structure

We report on the application of the SK scheme [10] to oxides having the simple cubic perovskite structure ABO_3. In this work our emphasis is on fitting the augmented plane wave (APW) band structure very well. Fitting of the total energies is not included here. In oxide materials the oxygen 2s-states are usually found to lie deep in the semicore states. These states are important for the accurate determination of the total energy of the system in first-principles calculations but they are not essential in a tight-binding description of the band structure. Therefore, the Hamiltonian size is in general 27×27 resulting from the s, p and d orbitals of the A and B atoms and the nine 2p orbitals of oxygen. The size of the Hamiltonian is reduced further depending upon the particular atoms A and B. In this section we present results for $KBiO_3$, $PbTiO_3$, $CaMnO_3$ and $LaMnO_3$. In previous work [11] we have discussed other perovskite TB parametrizations including spin-polarized systems [12,13].

3.1. $KBiO_3$

In Ref. [14] APW calculations for a lattice parameter $a = 8.11$ a.u. were reported together with TB–CPA results. In this work we have improved the quality of our TB fit. We have included in our TB Hamiltonian the 3p and 4s K orbitals, the s and p outer orbitals of Bi and the O 2p orbitals. Our secular equation is a 17×17 matrix and contains 29 parameters, two of which are oxygen second nearest-neighbor interactions as shown in Table 1. The fit was done with 35 k-points in the irreducible simple cubic Brillouin zone and has an rms deviation from the APW results of 11 mRy for the first 14 bands. The TB energy bands of $KBiO_3$ are shown in Fig. 3. The Fermi level, E_F, is denoted at zero energy with a broken line. The approximately 0.3 Ry wide manifold of bands below E_F is due to the O-2p states. Below the oxygen states there is a parabolic band that has predominantly Bi s-character. The narrow band at the bottom is due to the K-3p states. Above, but near, E_F we identify strong O p-character while in the top band (14th band) there is a mixture of K and Bi sp states. In the

Table 1
Slater–Koster parameters in Ry (A = K, Ca, La, Pb; B = Bi, Mn, Ti)

a_o (a.u)	$KBiO_3$ 8.11	$PbTiO_3$ 7.35	$CaMnO_3$ 7.35	$LaMnO_3$ 7.35
On-site energies				
A–A s	0.8825	0.1854	1.2946	1.3066
A–A p	−0.2815	0.9210	–	–
A–A t_{2g}	–	–	0.9112	0.8176
A–A e_g	–	–	0.9005	0.7899
B–B s	0.1474	–	1.1459	1.1873
B–B p	3.1387	–	–	–
B–B t_{2g}	–	0.7851	0.4534	0.4695
B–B e_g	–	0.8412	0.5563	0.5728
O–O p_x	0.3352	0.4554	0.2645	0.1998
O–O p_y,p_z	0.2928	0.3946	0.3654	0.2966
First-neighbor hopping integrals				
A–A ssσ	−0.0066	−0.0013	0.0247	0.0108
A–A spσ	−0.0363	0.0044	–	–
A–A ppσ	0.0024	0.0433	–	–
A–A ppπ	0.0023	−0.0019	–	–
A–A sdσ	–	–	−0.0020	0.0196
A–A ddσ	–	–	−0.0271	−0.0569
A–A ddπ	–	–	0.0034	0.0075
A–A ddδ	–	–	−0.0016	−0.0024
B–B ssσ	−0.0113	–	−0.0249	−0.0197
B–B spσ	−0.0489	–	–	–
B–B ppσ	0.3707	–	–	–
B–B ppπ	−0.1032	–	–	–
B–B sdσ	–	–	0.0229	0.0141
B–B ddσ	–	0.0153	−0.0095	−0.0112
B–B ddπ	–	−0.0022	−0.0030	−0.0062
B–B ddδ	–	−0.0155	−0.0001	−0.0014
O–O ppσ	0.0307	0.0443	0.0429	0.0350
O–O ppπ	−0.0016	−0.0024	−0.0075	−0.0046
A–B ssσ	−0.0017	–	−0.0350	−0.0403
A–B spσ	−0.0076	–	–	–
A–B ppσ	−0.0523	–	–	–
A–B ppπ	−0.0186	–	–	–
A–B sdσ	–	−0.0067	−0.0069	0.0204
A–B pdσ	–	−0.0637	–	–
A–B pdπ	–	0.0138	–	–
A–B ddσ	–	–	0.0204	0.0190
A–B ddπ	–	–	−0.0021	−0.0010
A–B ddδ	–	–	0.0039	0.0043
A–B psσ	−0.0001	–	–	–
A–B dsσ	–	–	−0.0176	−0.0194
A–O spσ	−0.0603	0.0605	–	–
A–O ppσ	−0.0064	0.0934	–	–
A–O ppπ	−0.0111	−0.0089	–	–
A–O dpσ	–	–	−0.0850	−0.1219
A–O dpπ	–	–	0.0312	0.0352
B–O spσ	−0.1559	–	−0.0227	−0.0785
B–O ppσ	0.3389	–	–	–
B–O ppπ	−0.0455	–	–	–
B–O dpσ	–	0.1568	0.1321	0.1309
B–O dpπ	–	−0.0627	−0.0670	−0.0677
Second-neighbor hopping integrals				
O–O ppσ	−0.0085	−0.0017	0.0072	0.0040
O–O ppπ	0.0041	0.0009	−0.0028	−0.0025

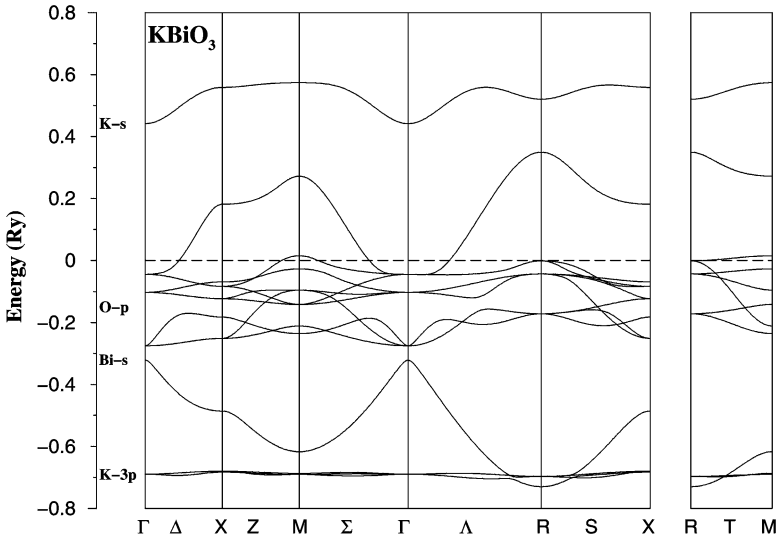

Fig. 3. Energy bands of the simple cubic perovskite material $KBiO_3$ showing metallic character.

late 1980s a $Ba_{1-x}K_xBiO_3$ compound (with $x = 0.4$) was found to display superconductivity with $T_c = 40$ K. Calculations by Mattheiss et al. [15] and by Papaconstantopoulos et al. [14] for this material and for the $BaPb_{1-y}Bi_yO_3$ system suggested an electron–phonon mechanism to explain superconductivity. A more detailed discussion on non-cuprate superconductors can be found in Pickett's article in this volume [16].

3.2. $PbTiO_3$

We first performed APW calculations at the LDA equilibrium value of 7.35 a.u reported in the pseudopotential calculations of King–Smith and Vanderbilt [17]. We then constructed our TB Hamiltonian, including the 6s and 6p Pb orbitals, the 3d-Ti orbitals, and the 2p O orbitals, resulting in an 18×18 secular equation containing 25 parameters, as shown in Table 1. The fitting error was 13 mRy for 16 bands. The energy bands are shown in Fig. 4. This band structure is very close to that given by Singh [18] using the full potential LAPW method. The valence and conduction bands are separated by a gap of approximately 0.19 Ry. The lowest band is due to the Pb 5s states and the remaining group of nine valence bands is derived from the O 2p states, with smaller contributions from the Ti 3d states. The above observations from the bands are better clarified by inspection of Fig. 5 which shows the total and decomposed densities of states. This figure shows that the Ti d states have their strongest contribution in the conduction band, where the oxygen participation is very small, while there is a significant Pb p-like component. Note also a significant Ti e_g contribution in the valence band and the prominent Pb s-like peak at the bottom of the valence band.

$PbTiO_3$ is one end of the technologically important alloy system PZT, i.e. $Pb(Zr,Ti)O_3$. The cubic perovskite $PbTiO_3$ undergoes a transition to a tetragonal phase below 493°C. While we cannot study the energetics of this transition with this TB Hamiltonian it should be possible to examine the band structure of the tetragonal phase. In Table 1 we have also included the SK parameters for $CaMnO_3$ and $LaMnO_3$. These parameters have been derived from APW calculations at a lattice constant of 7.35 a.u. in the hypothetical paramagnetic phase and produce an equally good fit as in the other compounds mentioned above. To describe the real materials, which are antiferromagnetic insulators [19], an adjustment to the on-site terms could be made to invoke the necessary difference between up and down bands as described in Ref. [19].

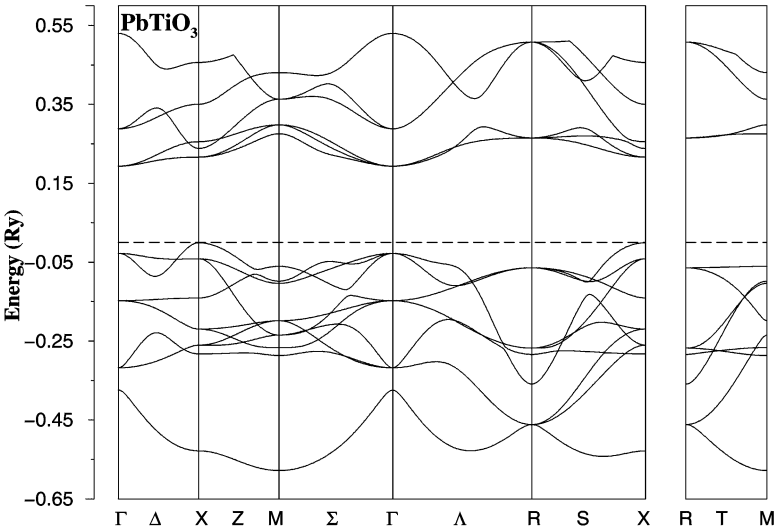

Fig. 4. Energy bands of $PbTiO_3$ in the simple cubic perovskite structure found to be an insulator.

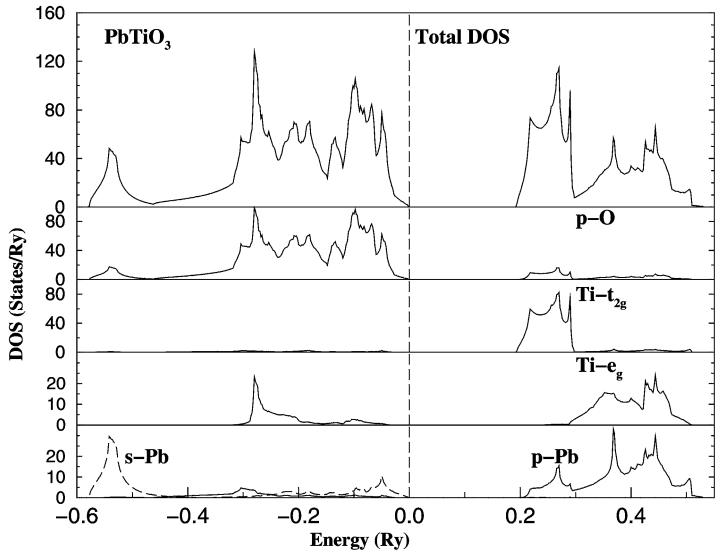

Fig. 5. Valence and conduction band densities of states of $PbTiO_3$ showing the total and various site and angular momentum decompositions.

4. Tight-binding calculations including spin–orbit coupling

The SK parametrizations presented in Ref. [5] do not include the spin–orbit coupling. For the heavier elements of the 5d series the addition of the spin–orbit interaction can cause significant changes in the band structure. We have recently [20] followed a procedure proposed by Hass et al. [21] which incorporates the spin–orbit effects within the tight-binding formalism. This approach results in a TB matrix that is dimensioned 18×18 in a typical

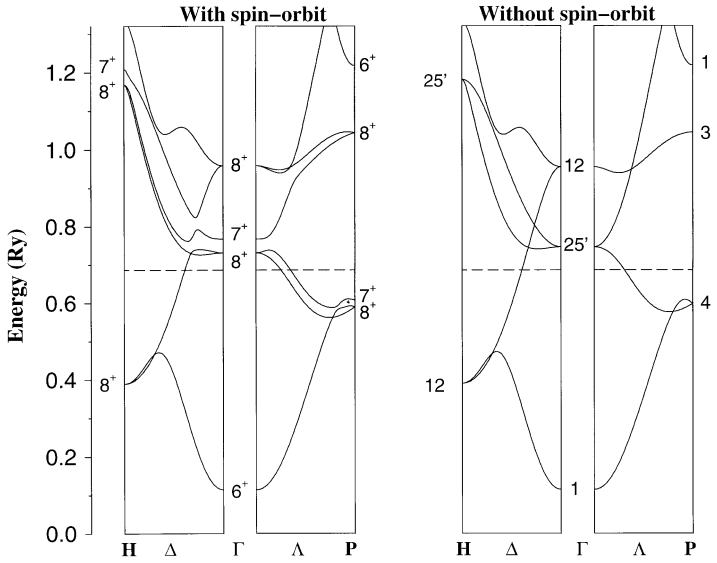

Fig. 6. Comparison of the energy bands of BCC Ta with and without spin–orbit interaction.

transition metal and has the form

$$\tilde{H} + \tilde{H}_{\mathrm{so}} = \begin{pmatrix} H + H_{\mathrm{so}}(\uparrow\uparrow) & H_{\mathrm{so}}(\uparrow\downarrow) \\ H_{\mathrm{so}}(\downarrow\uparrow) & H + H_{\mathrm{so}}(\downarrow\downarrow) \end{pmatrix}, \qquad (4.1)$$

where H is the usual 9×9 SK matrix and H_{so} is a matrix which contains the spin–orbit parameter λ. In our calculations the matrix H has the three-center non-orthogonal parameters given in Ref. [5]. For the parameter λ we have used the atomic values derived by Herman and Skillman [22] using perturbation theory. In general, we can consider two parameters corresponding to p and d orbitals. In practice, for the 5d metals we only need to consider the d spin–orbit parameter while for semiconductors or sp-metals we only include the p spin–orbit parameter. In Fig. 6 we show the band structure of Ta for two directions in the BCC Brillouin zone for which the effects of the spin–orbit interaction are important. The value of the d spin–orbit parameter from Ref. [22] is $\lambda = 0.0116$ Ry. At the Γ point the spin–orbit interaction splits the triply degenerate (in the single group) d-like $\Gamma_{25'}$ state into Γ_8^+ (fourfold degenerate) and Γ_7^+ (twofold degenerate) in the double group notation. The width of the splitting at Γ is 36 mRy. At the H point the state $H_{25'}$ splits in a similar way as at Γ with a width of 40 mRy. At the P point the triply degenerate P_4 state splits into P_8 (fourfold degenerate) and P_7 (twofold degenerate). The width of the splitting at P is 19 mRy. Similar splittings occur along the Δ and Λ directions for the doubly degenerate Δ_5 and Λ_3 states. There is no splitting due to spin orbit in the ΓN-(1 1 0) direction.

In Fig. 7 we give another example of the effects of spin orbit on the band structure of the FCC metal Pb. Again we use here the three-center non-orthogonal parameters of Ref. [5]. In the case of Pb the relevant spin–orbit parameter affects the p-like states and has, according to Ref. [22], the value 0.03119 Ry. We note from Fig. 7 that the triply degenerate p-like Γ_{15} state splits into Γ_8^- (fourfold degenerate) and Γ_6^- (twofold degenerate) with a width of 208 mRy. At the L point the doubly degenerate $L_{3'}$ state splits into L_4^- (twofold degenerate) and $L_5^- - L_6^-$ (twofold degenerate) with a width of 117 mRy. At the symmetry point X the doubly degenerate state $X_{5'}$ splits into the twofold degenerate states X_{6-} and X_{7-} with a width of 67 mRy. Finally, at the W point the doubly degenerate W_3 state splits into W_6 and W_7, both of which are twofold degenerate in the double group notation and have a width of 54 mRy. It is clear from Figs. 6 and 7 that for both Ta and Pb the

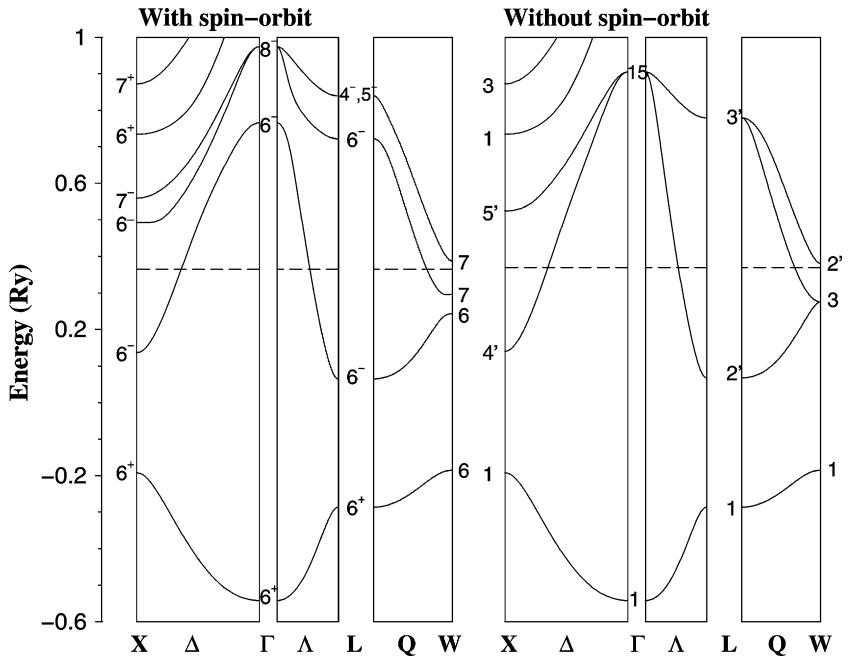

Fig. 7. Comparison of the energy bands of FCC Pb with and without spin–orbit interaction.

introduction of the spin–orbit interaction results in significant changes of the Fermi surface. In our future work we will provide a quantitative account of these changes.

5. Summary

In this article we first recollect the earlier work of Economou with DAP on Si and Si–H, and summarize the applications of the NRL–TB method presenting new results on possible FCC metastable phases of the BCC and HCP metals. In addition two new applications of the SK scheme are given. The first one is on a detailed and accurate fit of the band structure of cubic perovskites, and the second one describes examples of the inclusion of the spin–orbit interaction in tight-binding calculations.

Acknowledgements

This research was supported by the US Office of Naval Research. Development of the NRL–TB codes was partially supported by the US Department of Defense Common HPC Software Support Initiative (CHSSI).

References

[1] D.A. Papaconstantopoulos, E.N. Economou, Phys. Rev. B 22 (1980) 2903.
[2] E.N. Economou, D.A. Papaconstantopoulos, Phys. Rev. B 23 (1982) 2042.
[3] D.A. Papaconstantopoulos, E.N. Economou, Phys. Rev. B 24 (1983) 7233.
[4] W.E. Pickett, D.A. Papaconstantopoulos, E.N. Economou, Phys. Rev. B 28 (1983) 2232.
[5] D.A. Papaconstantopoulos, Handbook of the Band Structure of Elemental Solids, Plenum Press, New York, 1986.
[6] M.J. Mehl, D.A. Papaconstantopoulos, Phys. Rev. B 54 (1996) 4519.
[7] O.K. Andersen, Phys. Rev. B 12 (1975) 3060.
[8] N.C. Bacalis, D.A. Papaconstantopoulos, M.J. Mehl, M. Lach-hab, in this volume, Physica B 296 (2001) 125.
[9] P. Villars, L.D. Calvert, Pearson's Handbook of Crystallographic Data for Intermetallic Phases, 2nd Edition, ASM International, Materials Park, OH, 1991.
[10] J.C. Slater, G.F. Koster, Phys. Rev. 94 (1954) 1498.

[11] J.P. Julien, D.A. Papaconstantopoulos, D.J. Singh, W.E Pickett, F. Cyrot-Lackman, Physica C 220 (1994) 359.
[12] D.A. Papaconstantopoulos, W.E. Pickett, Phys. Rev. B 57 (1998) 12 751.
[13] I.I. Mazin, D.A. Papaconstantopoulos, D.J. Singh, Phys. Rev. B 61 (2000) 5233.
[14] D.A. Papaconstantopoulos, A. Pasturel, J.P. Julien, F. Cyrot-Lackmann, Phys. Rev. B 40 (1989) 8844.
[15] L.F. Mattheiss, E.M. Gyorgy, D.W. Johnson Jr., Phys. Rev. B 37 (1988) 3745.
[16] W.E. Pickett, in this volume, Physica B 296 (2001) 112.
[17] R.D. King-Smith, D. Vanderbilt, Phys. Rev. B 49 (1994) 5828.
[18] D.J. Singh, Phys. Rev. B 52 (1995) 12 559.
[19] W.E. Pickett, D.J. Singh, Phys. Rev. B 53 (1996) 1146.
[20] M. Lach-hab, D.A. Papaconstantopoulos, M.J. Mehl, J. Phys. Chem. Solids 61 (2000) 1639.
[21] K.C. Hass, H. Ehrenreich, B. Velicky, Phys. Rev. B 27 (1983) 1088.
[22] F. Herman, S. Skillman, Atomic Structure Calculations, Prentice-Hall, Englewood Cliffs, NJ, 1963.